Robust Image Filtering Using Joint Static and Dynamic Guidance Supplementary Material

Bumsub Ham[1,*] Minsu Cho[1,*] Jean Ponce[2,*]

[1]Inria [2]École Normale Supérieure / PSL Research University

1. Proof

Proposition 1. *$\Psi_\nu^y(x)$ is a surrogate function of $\psi_\nu(x)$.*

Proof. A function $g^y(x)$ is said to a surrogate function of $f(x)$ provided

$$\begin{cases} f(x) \leq g^y(x), \forall x, y \in [0, \infty) \\ f(y) = g^y(y), \forall y \in [0, \infty) \end{cases} . \tag{1}$$

Let us consider the following function:

$$f_\nu(x) = (1 - exp(-\nu x))/\nu. \tag{2}$$

Since $f_\nu''(x) < 0$, this function is strictly concave, $\forall x, y$,

$$f_\nu(x) \leq f_\nu(y) + (x - y) f_\nu'(y), \tag{3}$$

with equality holding at $x = y$. Thus, the surrogate function $g_\nu^y(x)$ is

$$\begin{aligned} g_\nu^y(x) &= f_\nu(y) + (x - y) f_\nu'(y) \\ &= f_\nu(y) + (x - y) exp(-\nu y) \\ &= f_\nu(y) + (x - y)(1 - \nu f_\nu(y)). \end{aligned} \tag{4}$$

Let us substitute x and y with x^2 and y^2, respectively, then

$$\begin{aligned} \psi_\nu(x) &= f_\nu(x^2) \\ &\leq g_\nu^{y^2}(x^2), \end{aligned} \tag{5}$$

and

$$\begin{aligned} g_\nu^{y^2}(x^2) &= f_\nu(y^2) + (x^2 - y^2)(1 - \nu f_\nu(y^2)) \\ &= \psi_\nu(y) + (x^2 - y^2)(1 - \nu \psi_\nu(y)) \\ &= \Psi_\nu^y(x). \end{aligned} \tag{6}$$

□

*WILLOW project-team, Département d'Informatique de l'Ecole Normale Supérieure, ENS/Inria/CNRS UMR 8548.

978-1-4673-6964-0/15/$31.00 ©2015 IEEE

2. More Results

Table 1. Quantitative Evaluation of Upsampled Depth Maps on the Middlebury Test Bed [8]

$\mathbf{u}^0 = \mathbb{1}$	*Tsukuba*		*Venus*		*Teddy*		*Cones*		*Art*	*Books*	*Dolls*	*Lau.*	*Moe.*	*Rei.*
Method	$\mathcal{O}_{all}$	$\mathcal{O}_{disc}$	$\mathcal{O}_{all}$	$\mathcal{O}_{disc}$	$\mathcal{O}_{all}$	$\mathcal{O}_{disc}$	$\mathcal{O}_{all}$	$\mathcal{O}_{disc}$	$\mathcal{O}_{all}$	$\mathcal{O}_{all}$	$\mathcal{O}_{all}$	$\mathcal{O}_{all}$	$\mathcal{O}_{all}$	$\mathcal{O}_{all}$
Bilinear Int.	10.40	46.30	3.29	37.10	11.80	35.30	14.60	35.80	34.59	13.07	14.59	22.85	17.15	17.48
GF [3]	9.87	43.20	2.74	26.50	15.50	37.50	15.50	34.40	45.31	19.14	19.64	26.89	22.22	21.70
Park et al. [6]	–	–	–	–	10.10	25.40	9.71	19.90	27.81	11.18	15.23	18.27	13.82	12.35
TGV [2]	5.40	23.90	1.31	14.40	9.82	29.00	10.20	23.60	23.59	13.14	16.14	15.12	18.26	10.42
WMF [5]	6.14	28.00	1.03	10.10	7.88	22.20	8.10	19.20	22.13	**8.67**	**9.58**	14.26	10.52	10.04
Ours	**2.39**	**10.40**	**0.55**	**5.10**	**7.39**	**20.30**	**5.24**	**12.40**	**10.04**	9.79	10.84	**8.11**	**9.49**	**6.93**

References

[1] Z. Farbman, R. Fattal, D. Lischinski, and R. Szeliski. Edge-preserving decompositions for multi-scale tone and detail manipulation. *ACM TOG*, 2008.

[2] D. Ferstl, C. Reinbacher, R. Ranftl, M. Rüther, and H. Bischof. Image guided depth upsampling using anisotropic total generalized variation. *in Proc. ICCV*, 2013.

[3] K. He, J. Sun, and X. Tang. Guided image filtering. *in Proc. ECCV*, 2010.

[4] L. Karacan, E. Erdem, and A. Erdem. Structure-preserving image smoothing via region covariances. *ACM TOG*, 2013.

[5] Z. Ma, K. He, Y. Wei, J. Sun, and E. Wu. Constant time weighted median filtering for stereo matching and beyond. *in Proc. ICCV*, 2013.

[6] J. Park, H. Kim, Y.-W. Tai, M. S. Brown, and I. Kweon. High quality depth map upsampling for 3d-tof cameras. *in Proc. ICCV*, 2011.

[7] G. Petschnigg, R. Szeliski, M. Agrawala, M. Cohen, H. Hoppe, and K. Toyama. Digital photography with flash and no-flash image pairs. *ACM TOG*, 2004.

[8] D. Scharstein and R. Szeliski. A taxonomy and evaluation of dense two-frame stereo correspondence algorithms. *IJCV*, 2002.

[9] L. Xu, Q. Yan, Y. Xia, and J. Jia. Structure extraction from texture via relative total variation. *ACM TOG*, 2012.

[10] Q. Yan, X. Shen, L. Xu, S. Zhuo, X. Zhang, L. Shen, and J. Jia. Cross-field joint image restoration via scale map. *in Proc. ICCV*, 2013.

[11] Q. Zhang, X. Shen, L. Xu, and J. Jia. Rolling guidance filter. *in Proc. ECCV*, 2014.

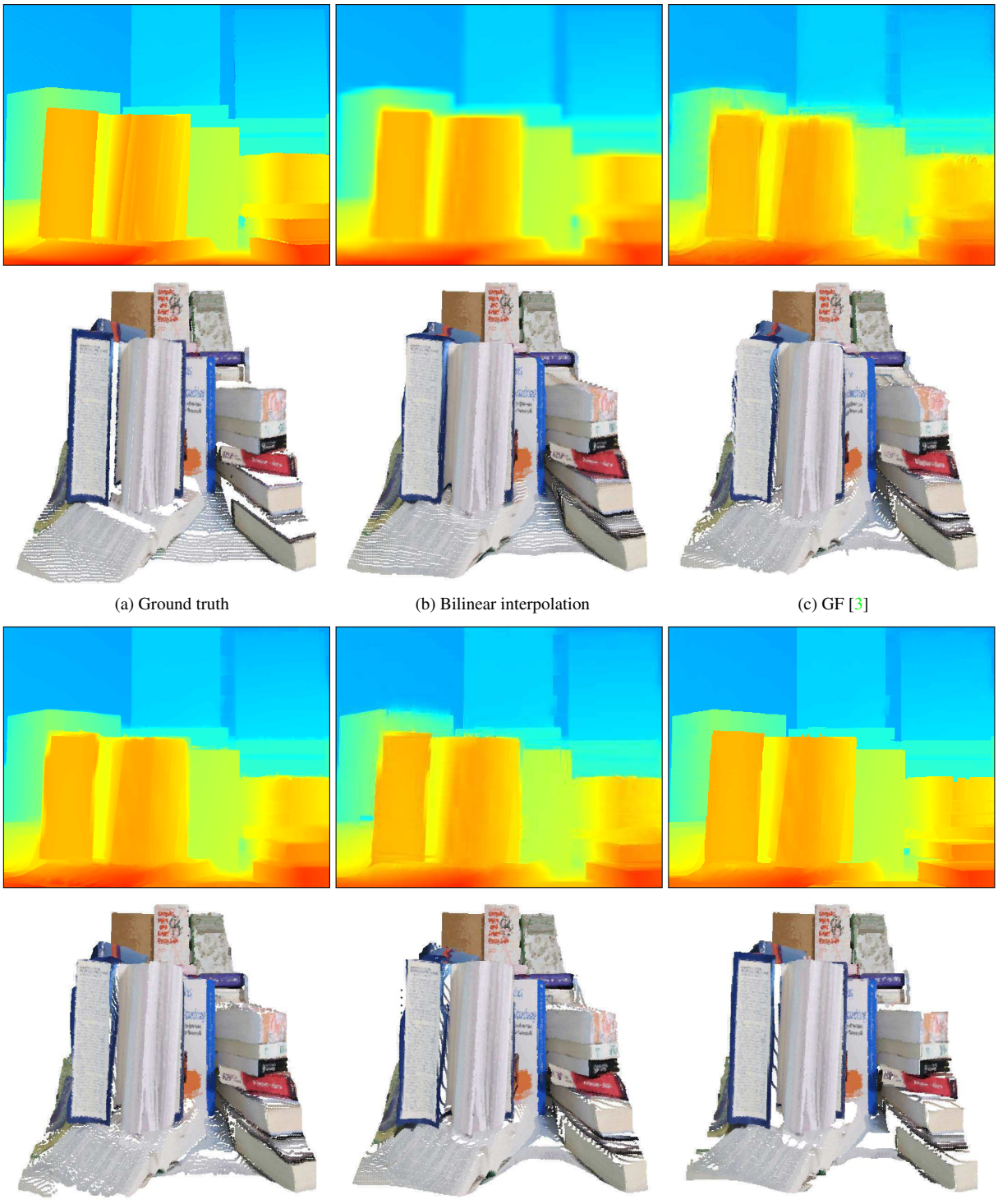

(a) Ground truth (b) Bilinear interpolation (c) GF [3]

(d) WMF [5] (e) TGV [2] (f) Ours

Figure 1. Visual comparison of ($\times 8$) upsampled depth maps and point cloud reconstructions on *books* sequence in the Middlebury test bed [8].

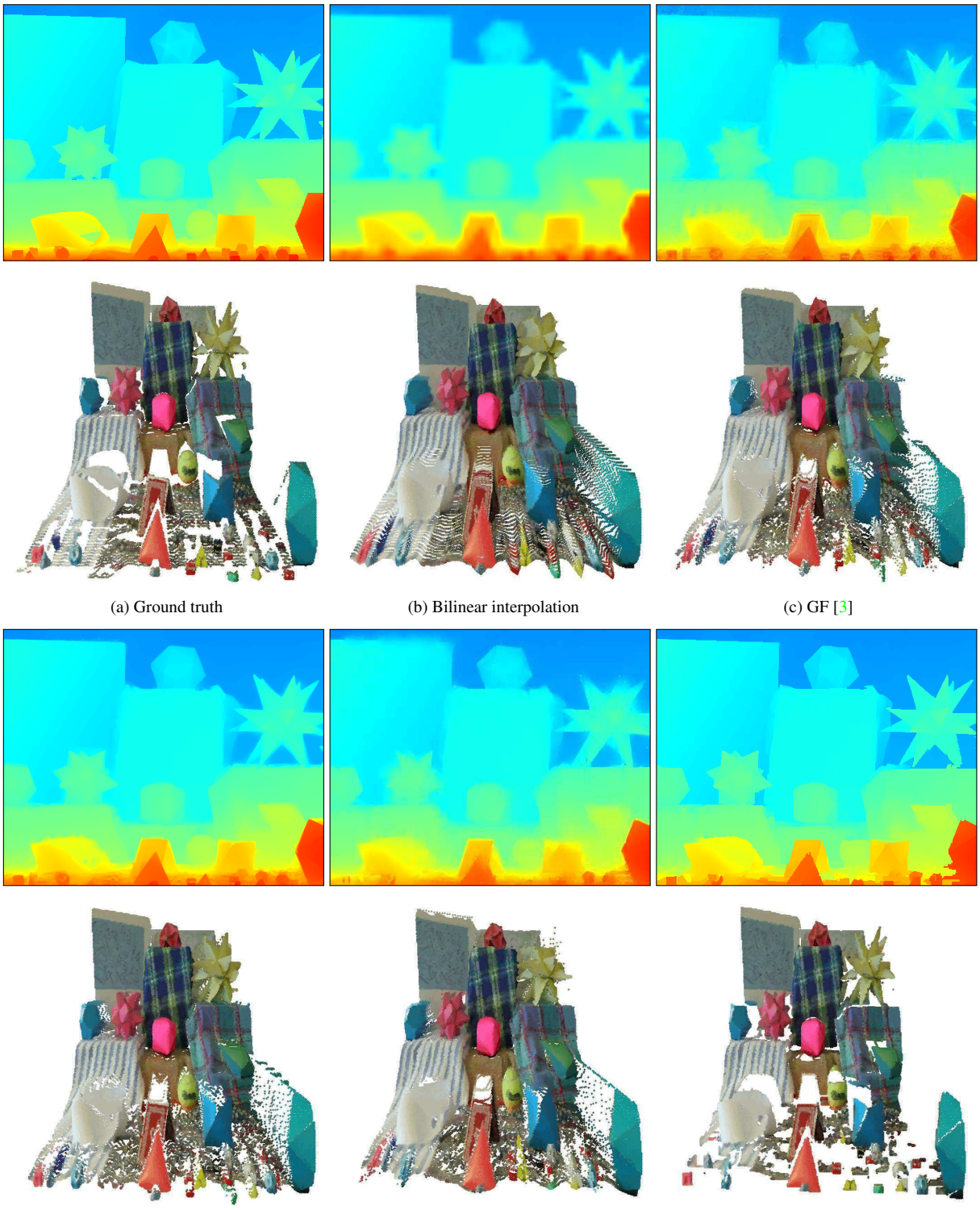

(a) Ground truth (b) Bilinear interpolation (c) GF [3]

(d) WMF [5] (e) TGV [2] (f) Ours

Figure 2. Visual comparison of ($\times 8$) upsampled depth maps and point cloud reconstructions on *moebius* sequence in the Middlebury test bed [8].

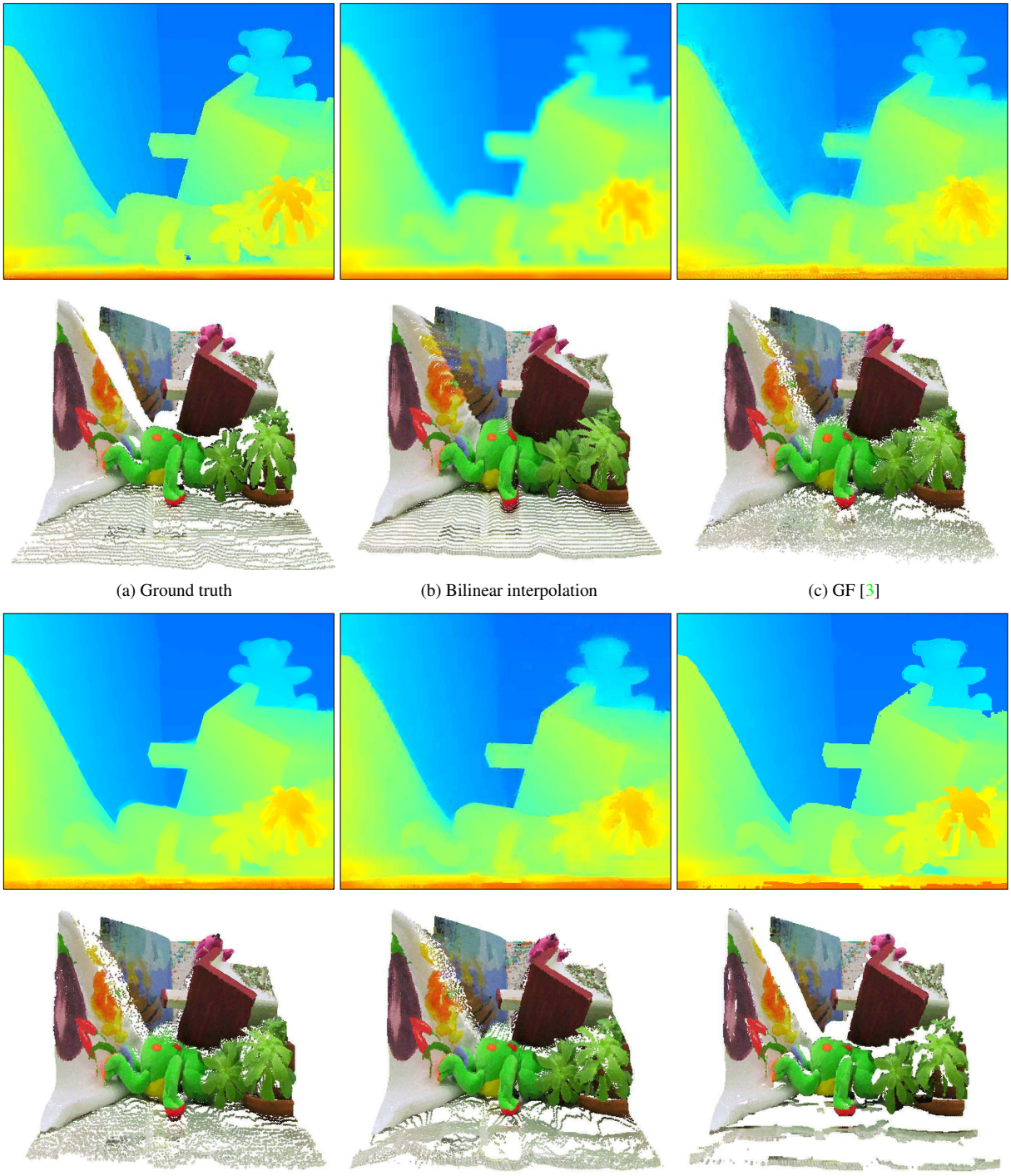

(a) Ground truth (b) Bilinear interpolation (c) GF [3]

(d) WMF [5] (e) TGV [2] (f) Ours

Figure 3. Visual comparison of ($\times 8$) upsampled depth maps and point cloud reconstructions on *teddy* sequence in the Middlebury test bed [8].

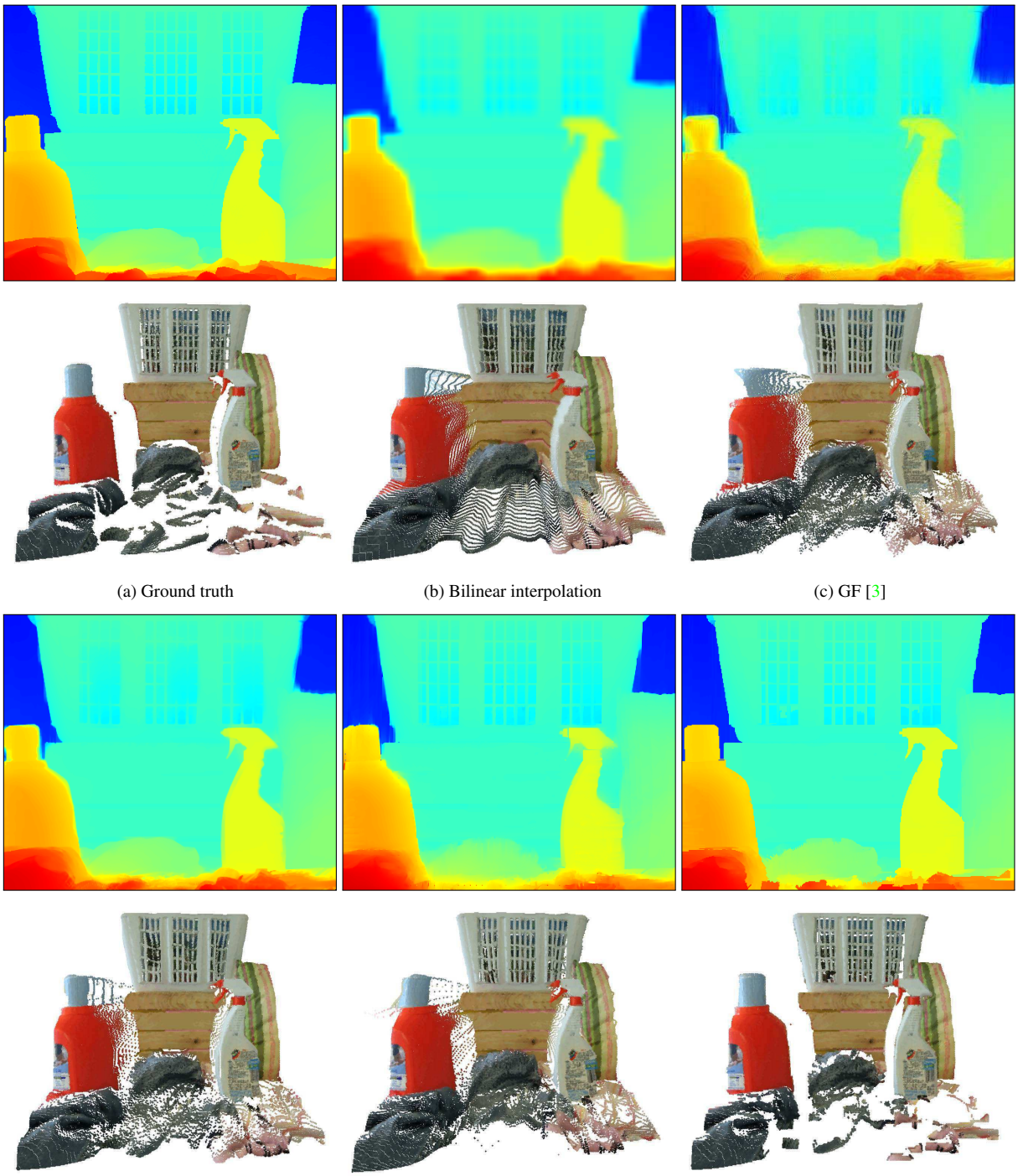

(a) Ground truth (b) Bilinear interpolation (c) GF [3]

(d) WMF [5] (e) TGV [2] (f) Ours

Figure 4. Visual comparison of ($\times 8$) upsampled depth maps and point cloud reconstructions on *laundry* sequence in the Middlebury test bed [8].

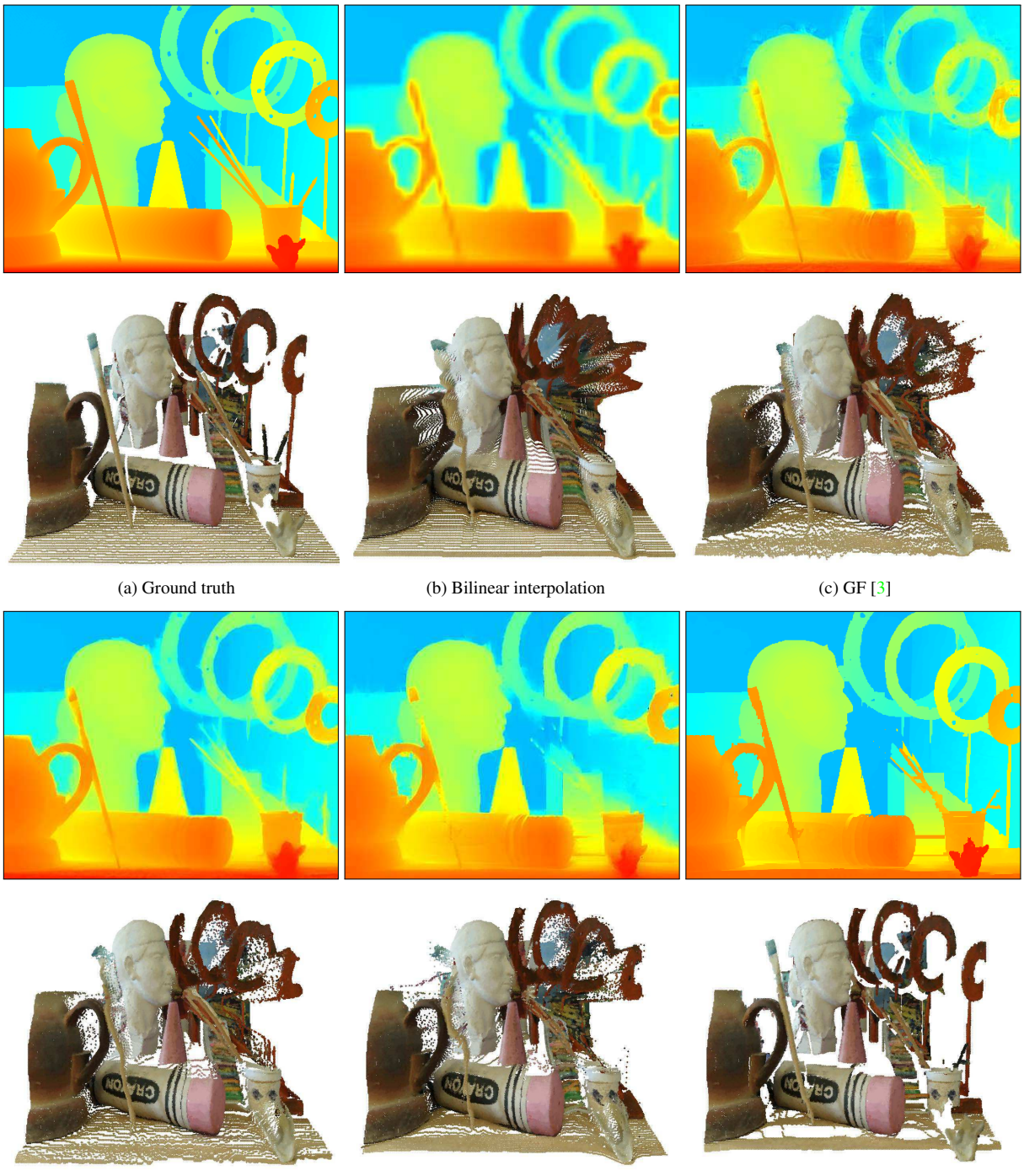

(a) Ground truth (b) Bilinear interpolation (c) GF [3]

(d) WMF [5] (e) TGV [2] (f) Ours

Figure 5. Visual comparison of ($\times 8$) upsampled depth maps and point cloud reconstructions on *art* sequence in the Middlebury test bed [8].

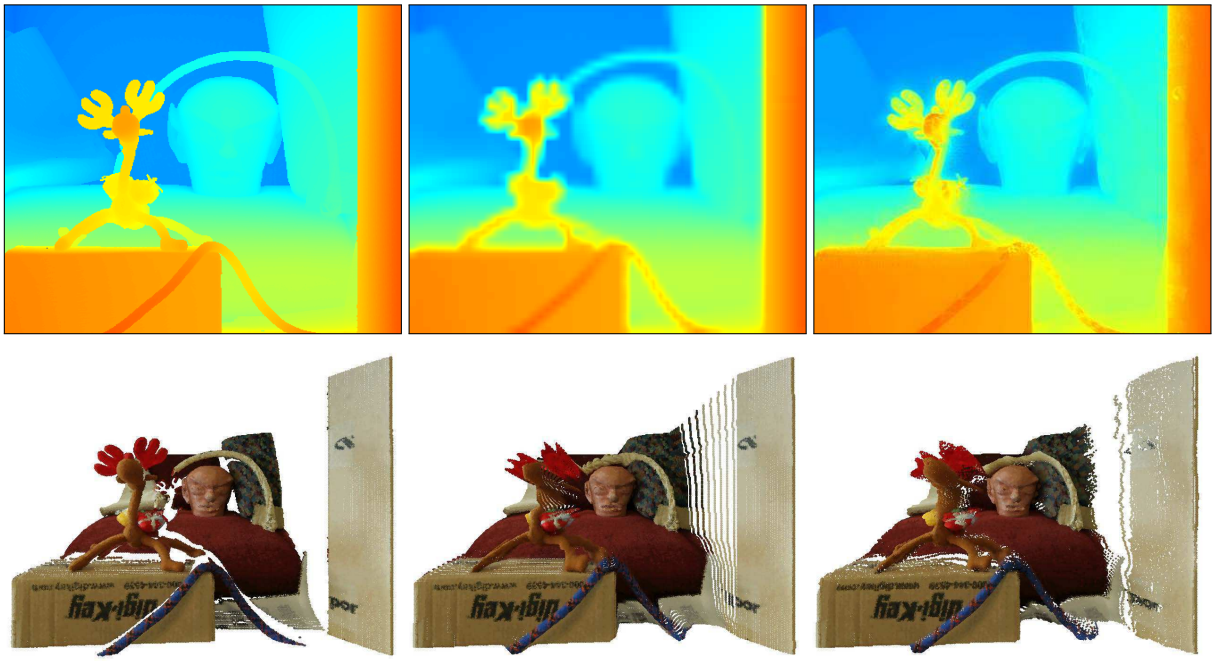

(a) Ground truth (b) Bilinear interpolation (c) GF [3]

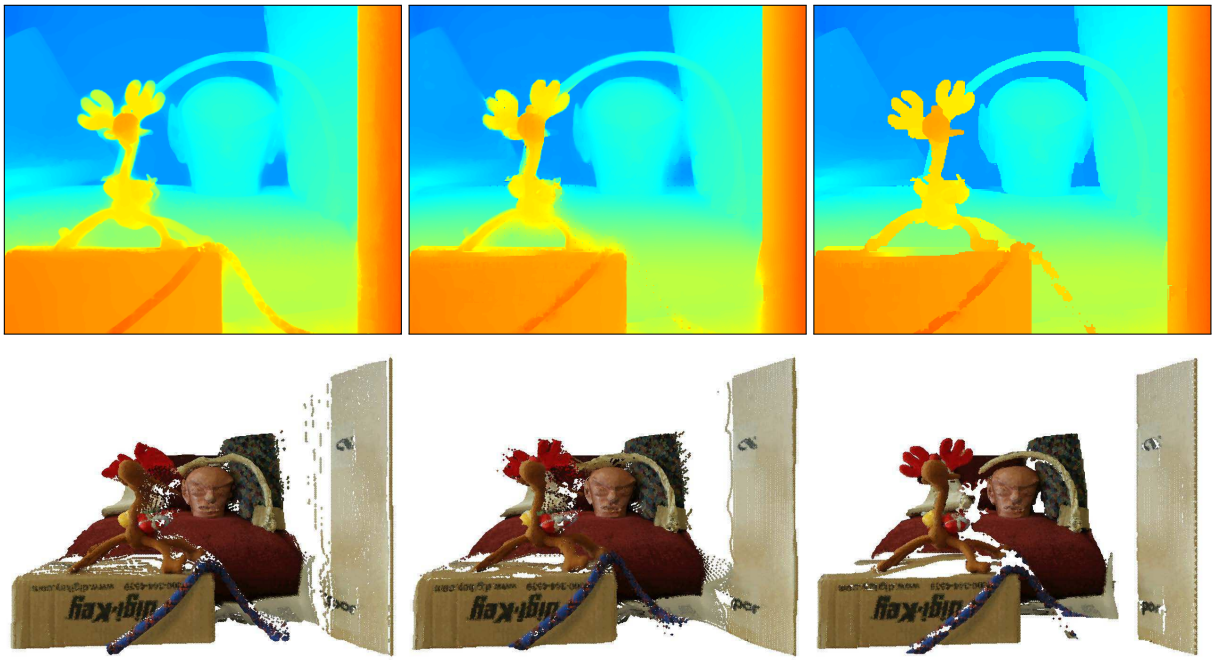

(d) WMF [5] (e) TGV [2] (f) Ours

Figure 6. Visual comparison of ($\times 8$) upsampled depth maps and point cloud reconstructions on *reindeer* sequence in the Middlebury test bed [8].

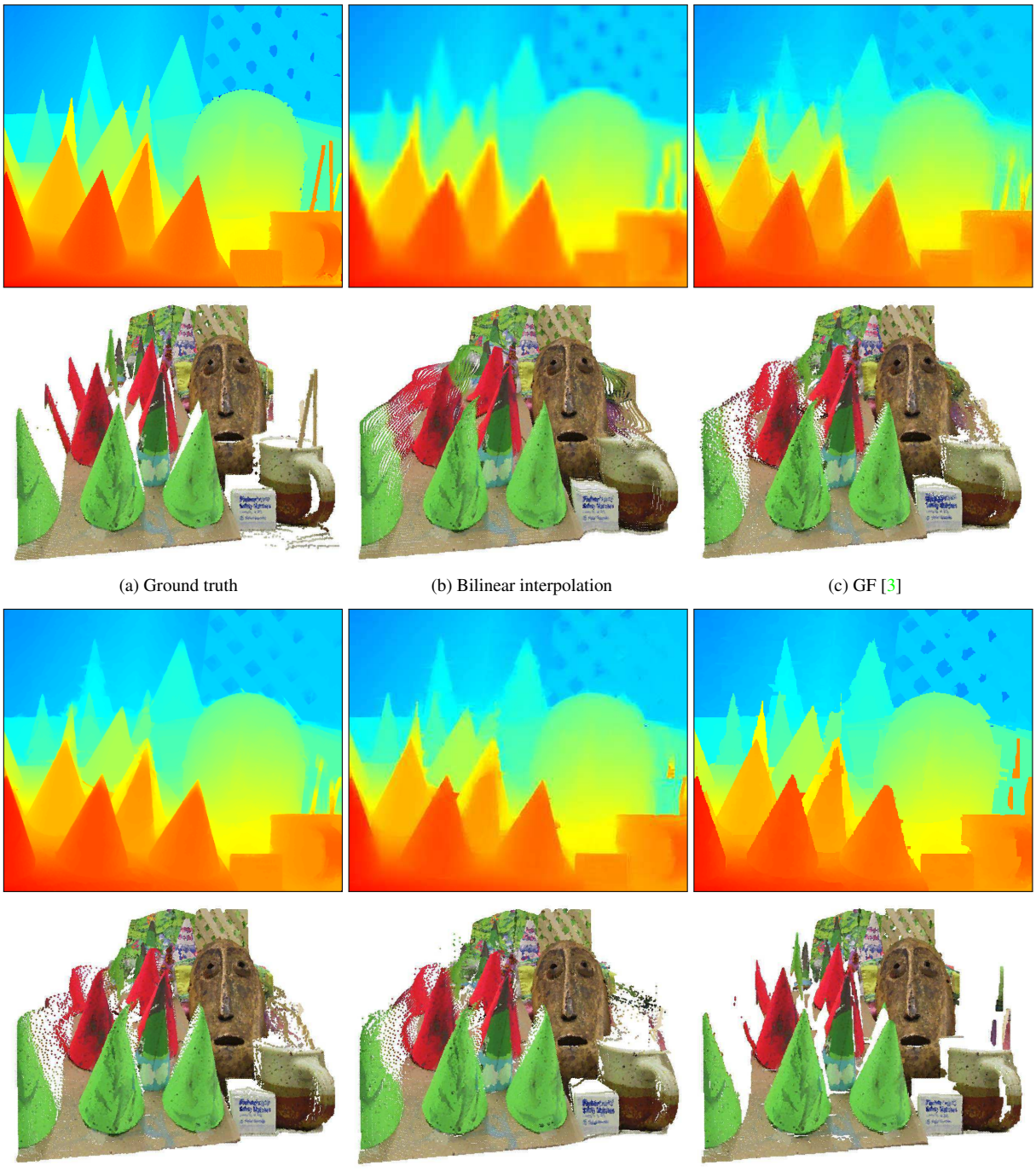

(a) Ground truth (b) Bilinear interpolation (c) GF [3]

(d) WMF [5] (e) TGV [2] (f) Ours

Figure 7. Visual comparison of ($\times 8$) upsampled depth maps and point cloud reconstructions on *cones* sequence in the Middlebury test bed [8].

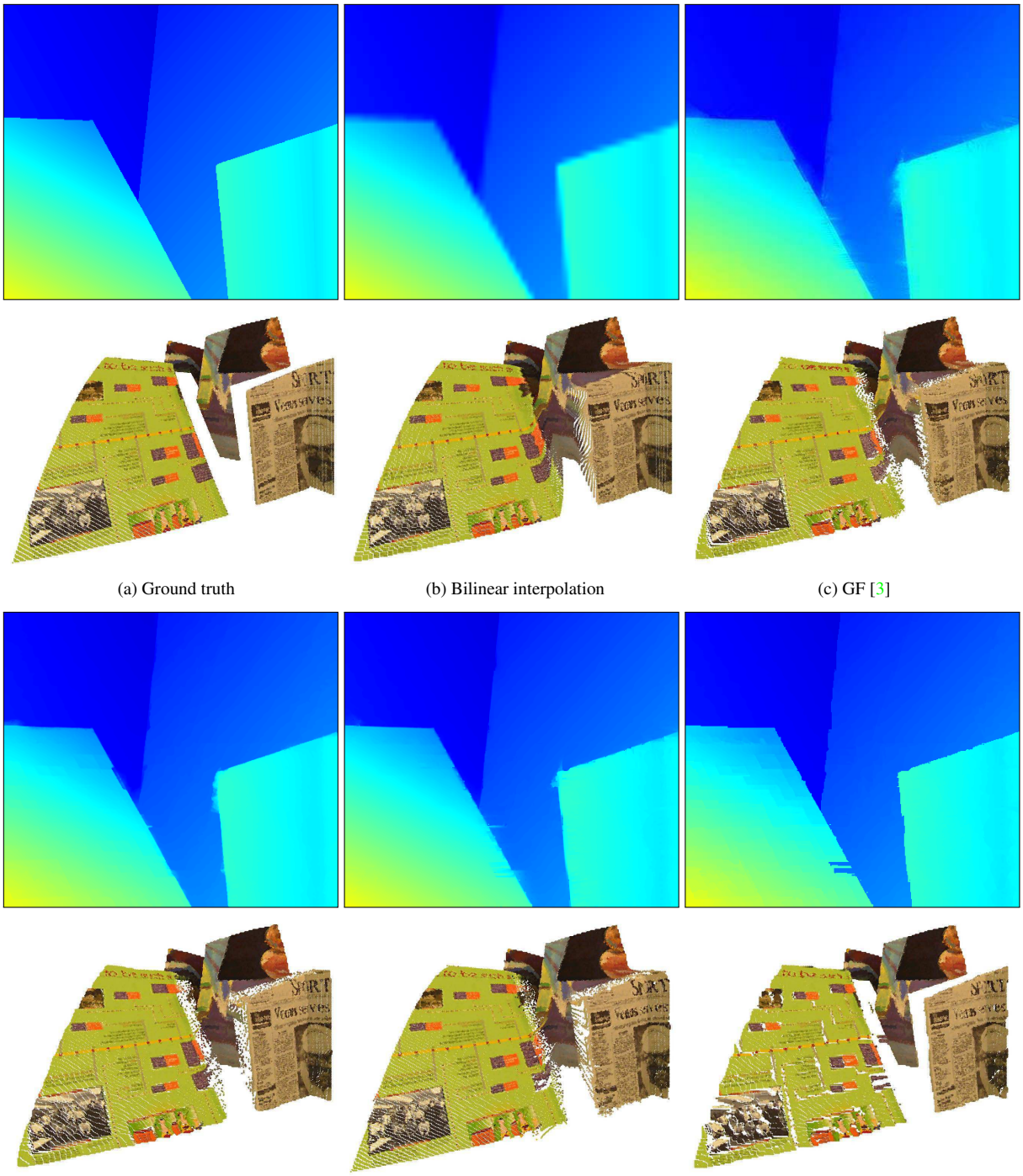

(a) Ground truth (b) Bilinear interpolation (c) GF [3]

(d) WMF [5] (e) TGV [2] (f) Ours

Figure 8. Visual comparison of ($\times 8$) upsampled depth maps and point cloud reconstructions on *venus* sequence in the Middlebury test bed [8].

(a) Intensity image

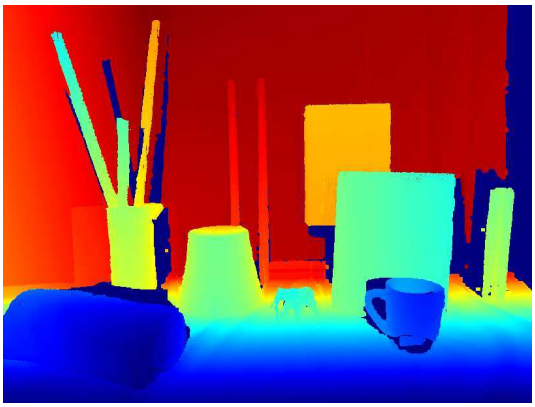

(b) Ground truth

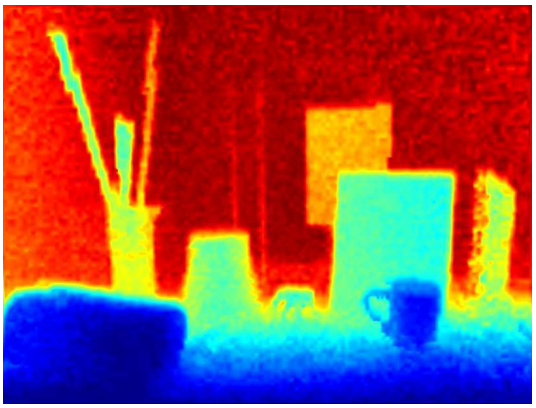

(c) Bilinear interpolation

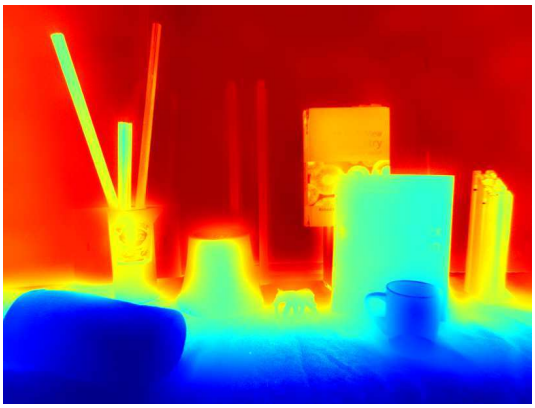

(d) GF [3]

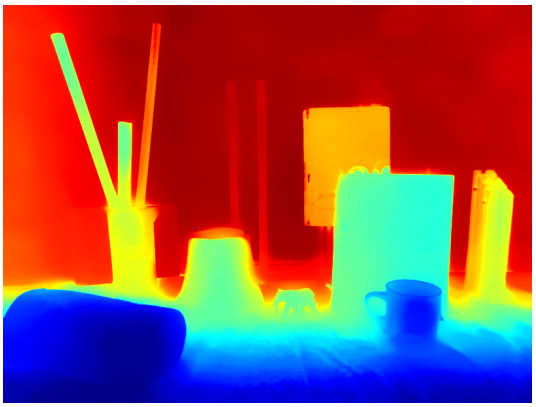

(e) WMF [5]

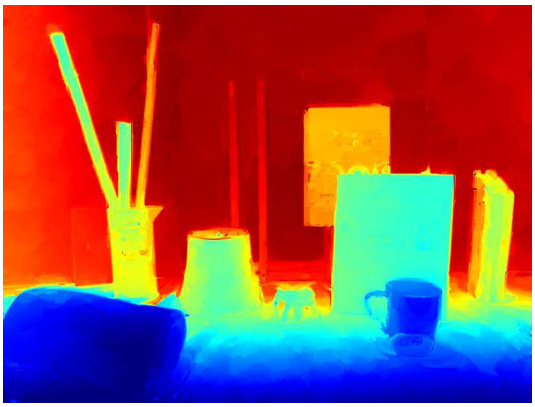

(f) TGV [2]

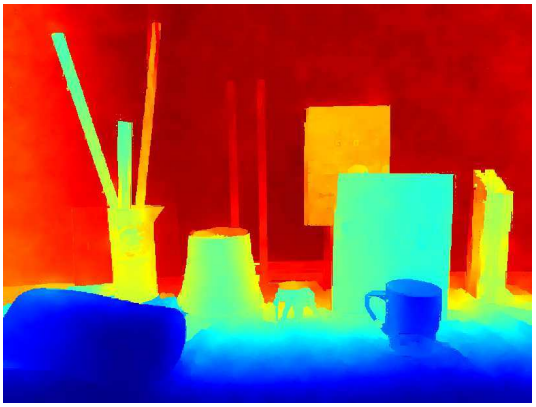

(g) Ours ($\lambda = 5$)

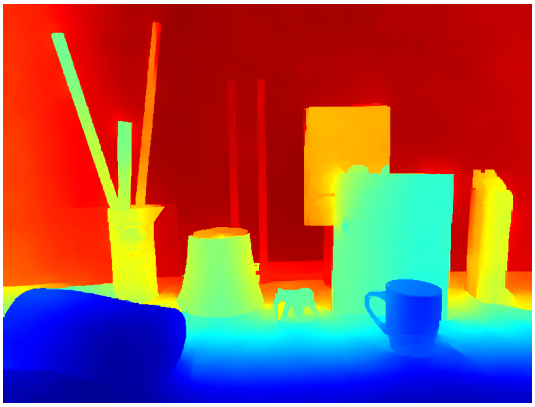

(h) Ours ($\lambda = 20$)

Figure 9. Visual comparison of upsampled depth maps on *books* sequence in the Graz data sets [2].

(a) Intensity image

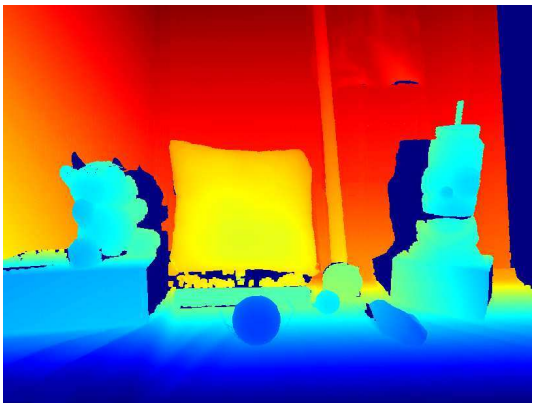

(b) Ground truth

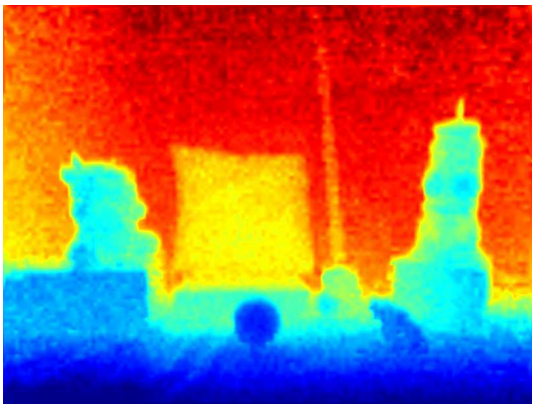

(c) Bilinear interpolation

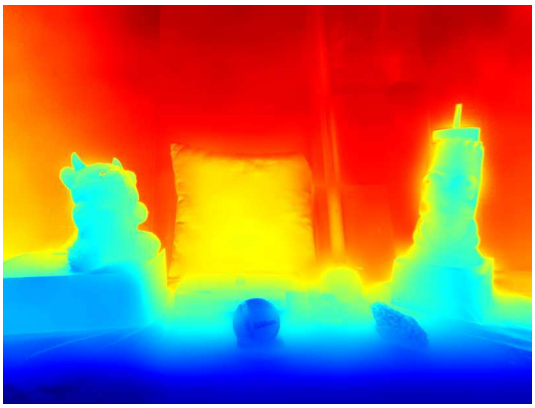

(d) GF [3]

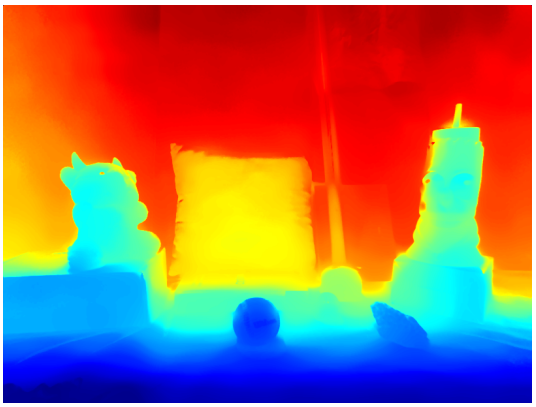

(e) WMF [5]

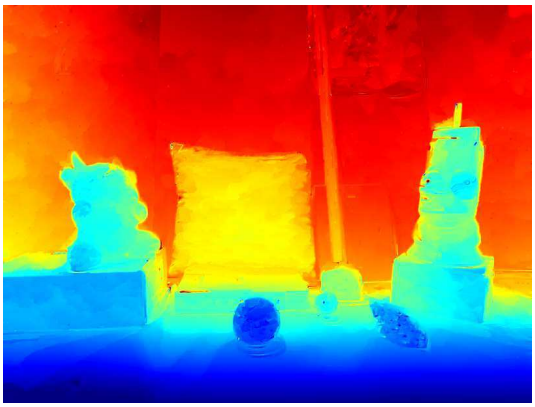

(f) TGV [2]

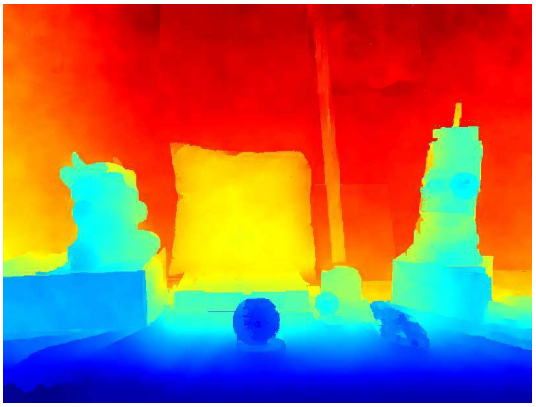

(g) Ours ($\lambda = 5$)

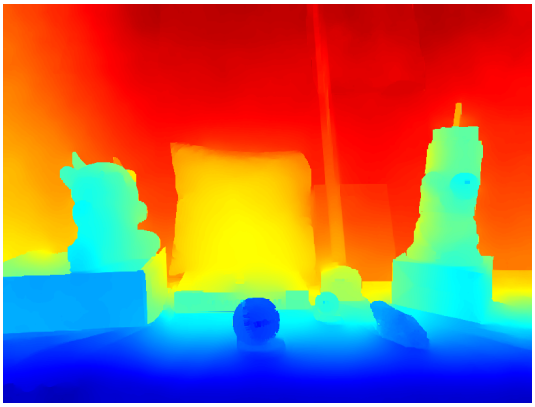

(h) Ours ($\lambda = 20$)

Figure 10. Visual comparison of upsampled depth maps on *devil* sequence in the Graz data sets [2].

(a) Intensity image

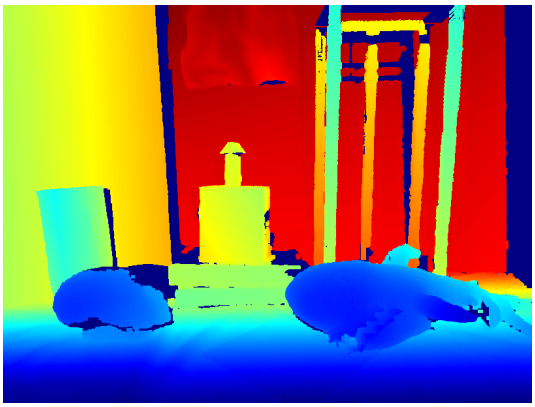

(b) Ground truth

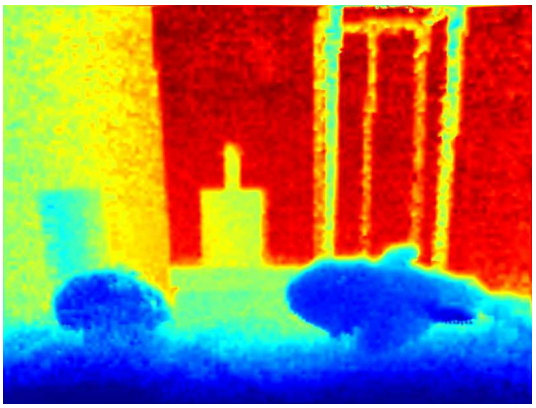

(c) Bilinear interpolation

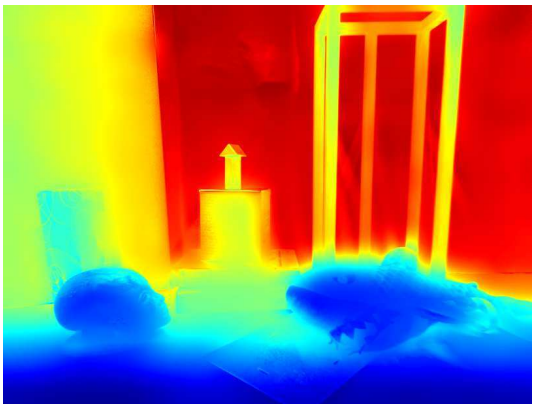

(d) GF [3]

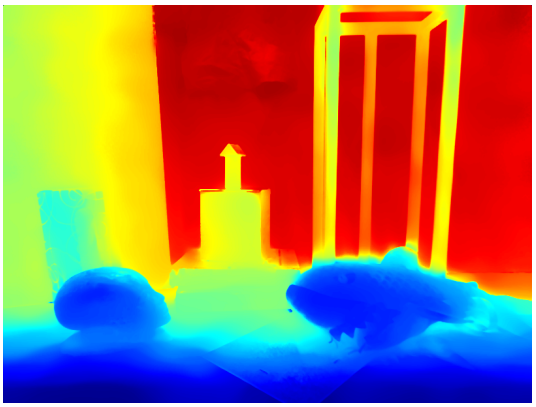

(e) WMF [5]

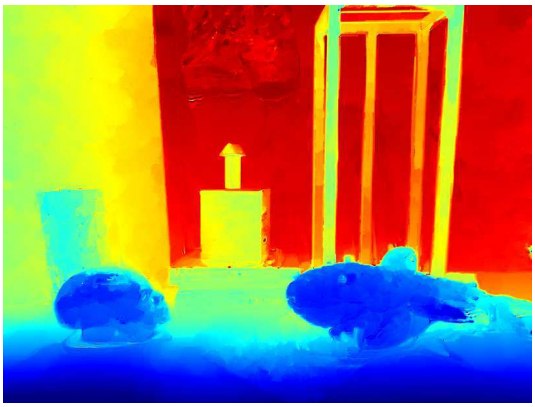

(f) TGV [2]

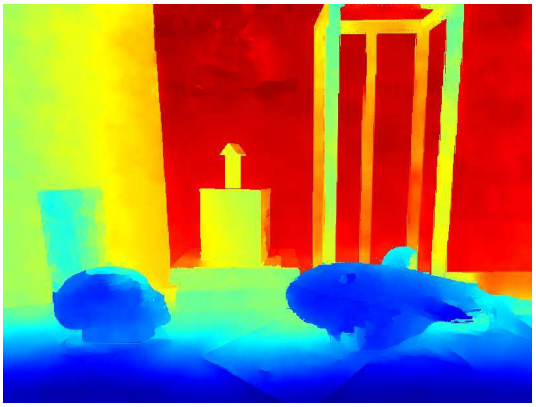

(g) Ours ($\lambda = 5$)

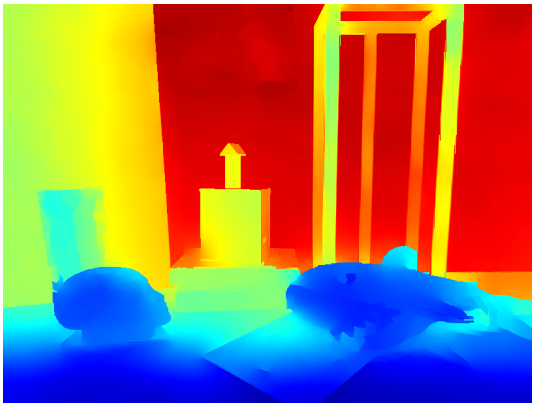

(h) Ours ($\lambda = 20$)

Figure 11. Visual comparison of upsampled depth maps on *shark* sequence in the Graz data sets [2].

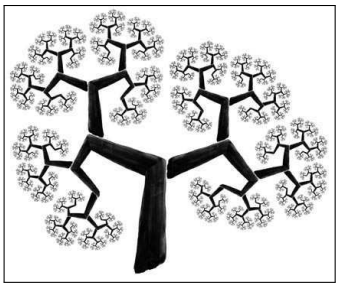

(a) Input image

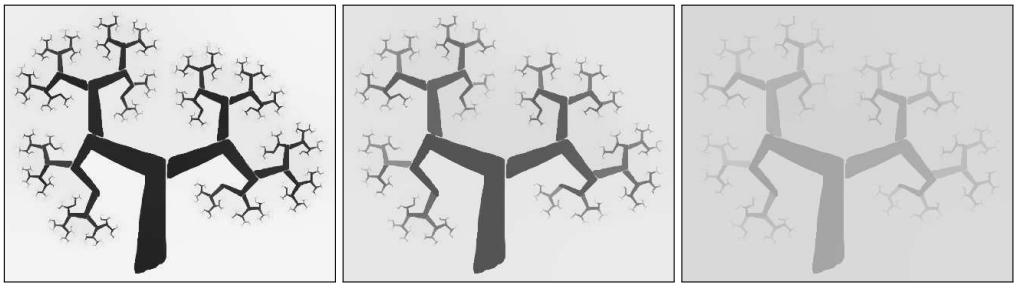

(b) WLS [1] ($\mu = 40$)

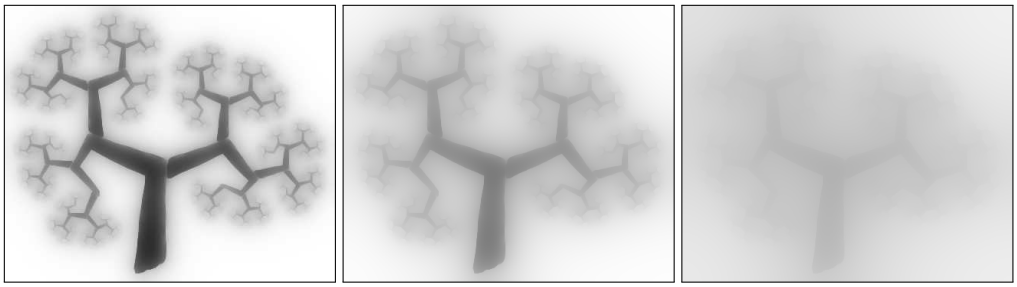

(c) WLS [1] ($\mu = 5$)

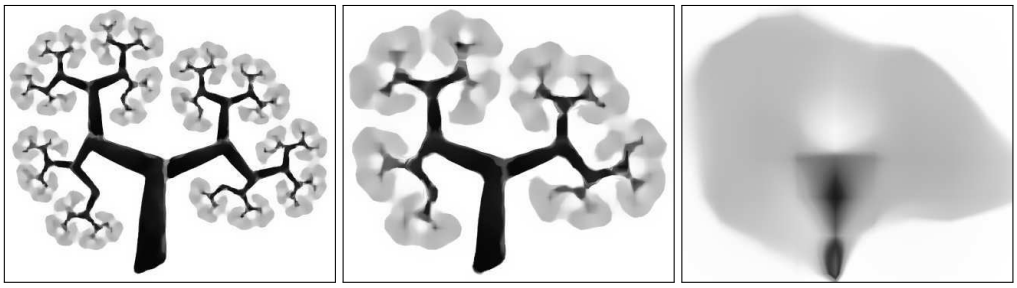

(d) RGF [11]

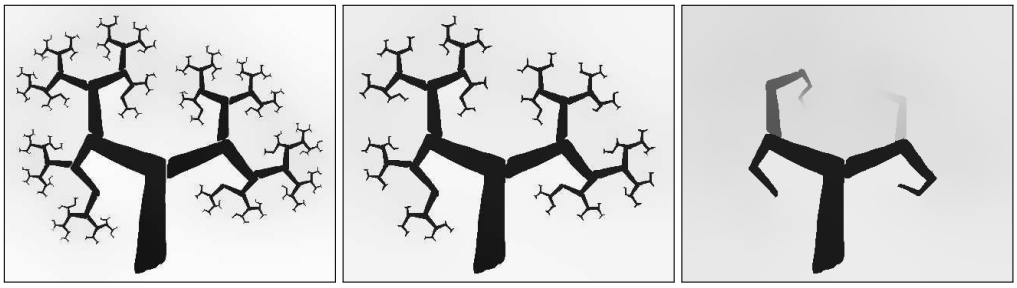

(e) Ours

Figure 12. Examples of the scale space for (a) the input image, constructed by (b) WLS [1] [(from left to right) $\lambda = 5\times10^3, 3\times10^4, 2\times10^5$, $\mu = 40$], (c) WLS [1] [(from left to right) $\lambda = 5 \times 10, 3 \times 10^2, 2 \times 10^3$, $\mu = 5$], (d) RGF [11] [(from left to right) $\sigma_s = 5, 10, 50$, $\sigma_r = 0.05$, $k = 5$], (e) our model [$\mathbf{u}^0 = \mathbf{u}_{l_1}$, (from left to right) $\lambda = 1 \times 10^3, 3 \times 10^3, 1 \times 10^4$, $\mu = 5$, $\nu = 40$, $k = 5$].

(a) Input image

(b) WLS [1] ($\mu = 40$)

(c) WLS [1] ($\mu = 5$)

(d) RGF [11]

(e) Ours

Figure 13. Examples of the scale space for (a) the input image, constructed by (b) WLS [1] [(from left to right) $\lambda = 5\times10^3, 3\times10^4, 4\times10^5$, $\mu = 40$], (c) WLS [1] [(from left to right) $\lambda = 5 \times 10, 3 \times 10^2, 4 \times 10^3$, $\mu = 5$], (d) RGF [11] [(from left to right) $\sigma_s = 5, 10, 100$, $\sigma_r = 0.05$, $k = 5$], (e) our model [$\mathbf{u}^0 = \mathbf{u}_{l_1}$, (from left to right) $\lambda = 3 \times 10^2, 1 \times 10^3, 4 \times 10^3$, $\mu = 5$, $\nu = 40$, $k = 5$].

(a) Input image

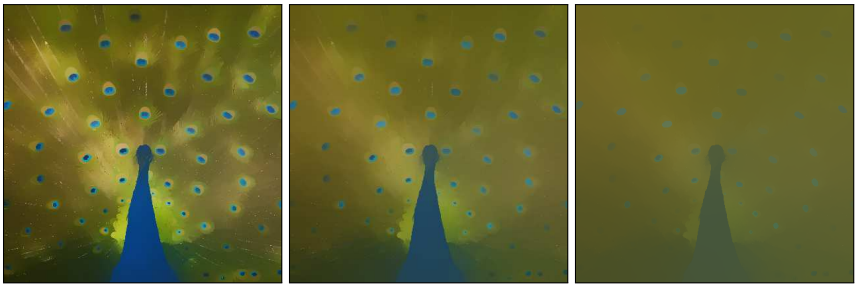

(b) WLS [1] ($\mu = 40$)

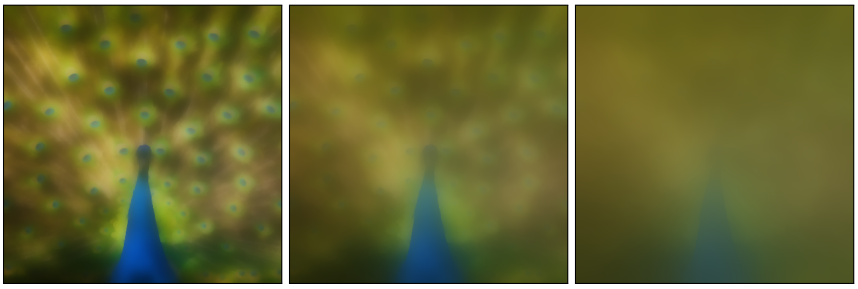

(c) WLS [1] ($\mu = 5$)

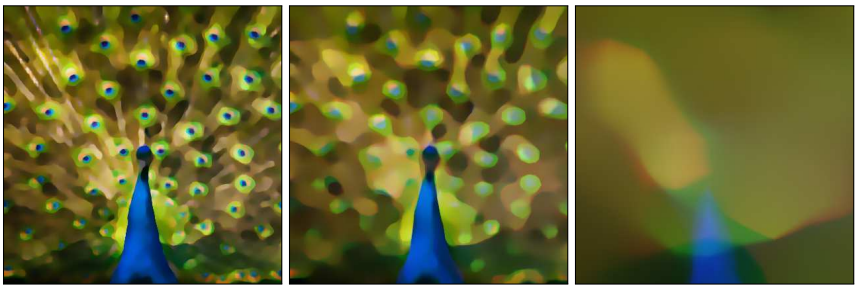

(d) RGF [11]

(e) Ours

Figure 14. Examples of the scale space for (a) the input image, constructed by (b) WLS [1] [(from left to right) $\lambda = 5\times10^3, 3\times10^4, 2\times10^5$, $\mu = 40$], (c) WLS [1] [(from left to right) $\lambda = 5 \times 10, 3 \times 10^2, 2 \times 10^3$, $\mu = 5$], (d) RGF [11] [(from left to right) $\sigma_s = 5, 10, 50$, $\sigma_r = 0.05$, $k = 5$], (e) our model [$\mathbf{u}^0 = \mathbf{u}_{l_1}$, (from left to right) $\lambda = 5 \times 10, 3 \times 10^2, 1 \times 10^4$, $\mu = 5$, $\nu = 40$, $k = 5$].

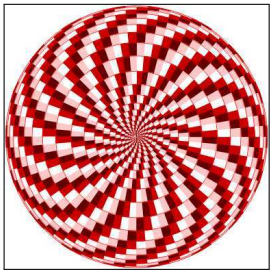

(a) Input image

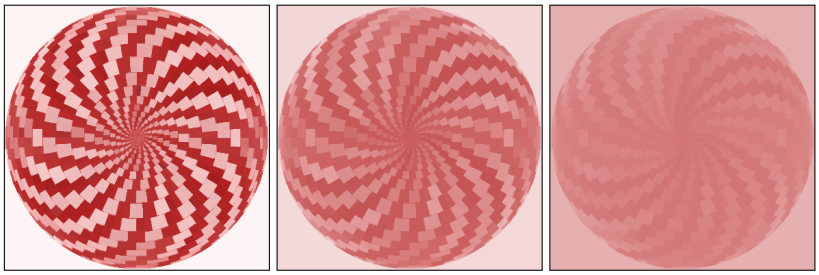

(b) WLS [1] ($\mu = 40$)

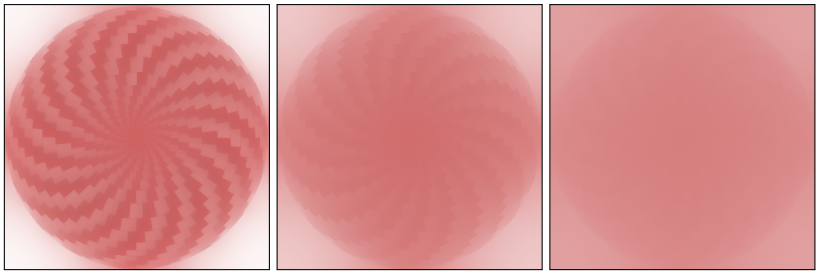

(c) WLS [1] ($\mu = 5$)

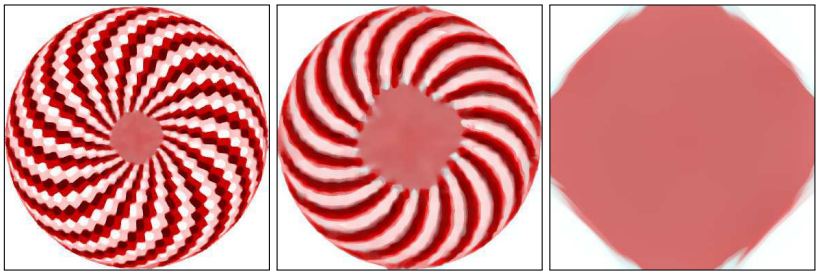

(d) RGF [11]

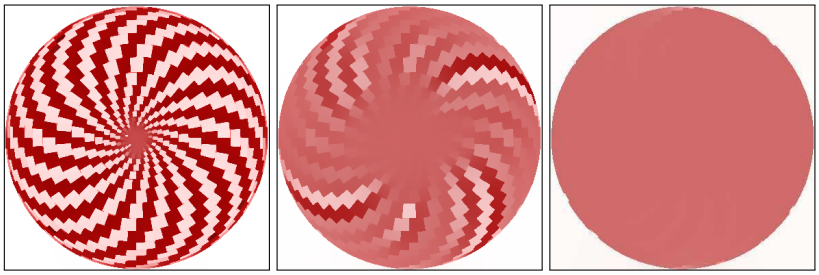

(e) Ours

Figure 15. Examples of the scale space for (a) the input image, constructed by (b) WLS [1] [(from left to right) $\lambda = 3\times10^4, 2\times10^5, 1\times10^6$, $\mu = 40$], (c) WLS [1] [(from left to right) $\lambda = 3 \times 10^2, 2 \times 10^3, 1 \times 10^4$, $\mu = 5$], (d) RGF [11] [(from left to right) $\sigma_s = 5, 10, 50$, $\sigma_r = 0.05$, $k = 5$], (e) our model [$\mathbf{u}^0 = \mathbb{1}$, (from left to right) $\lambda = 3 \times 10^2, 2 \times 10^3, 1 \times 10^4$, $\mu = 5$, $\nu = 40$, $k = 5$].

(a) Input image

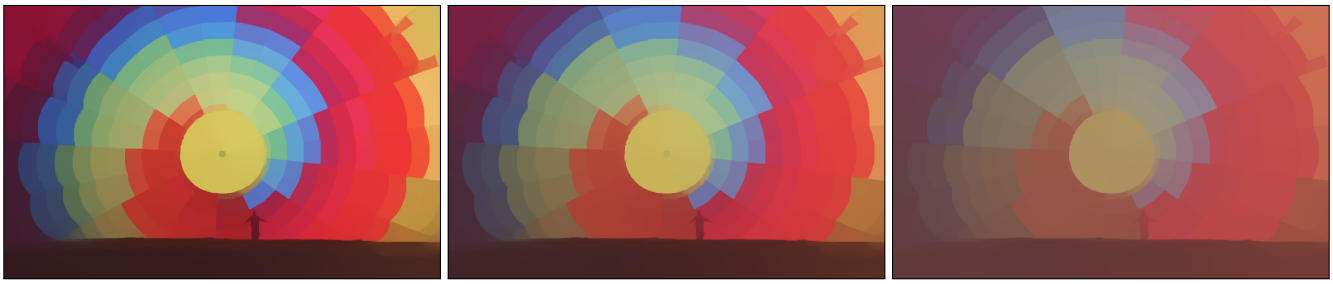

(b) WLS [1] ($\mu = 40$)

(c) WLS [1] ($\mu = 5$)

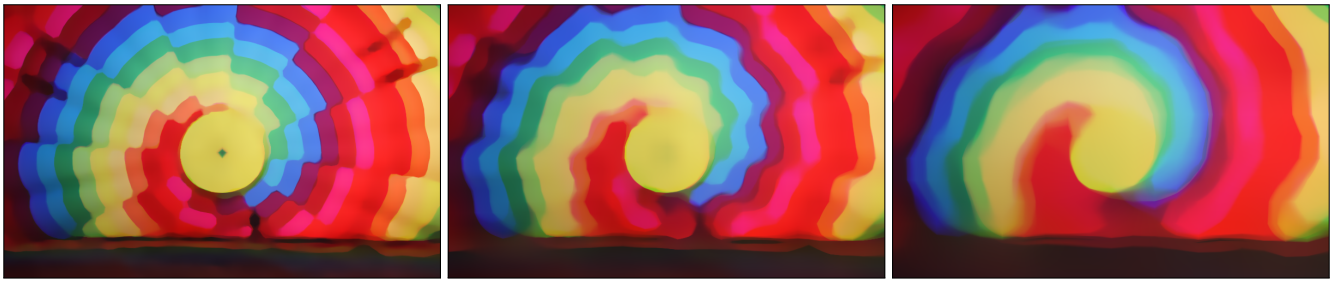

(d) RGF [11]

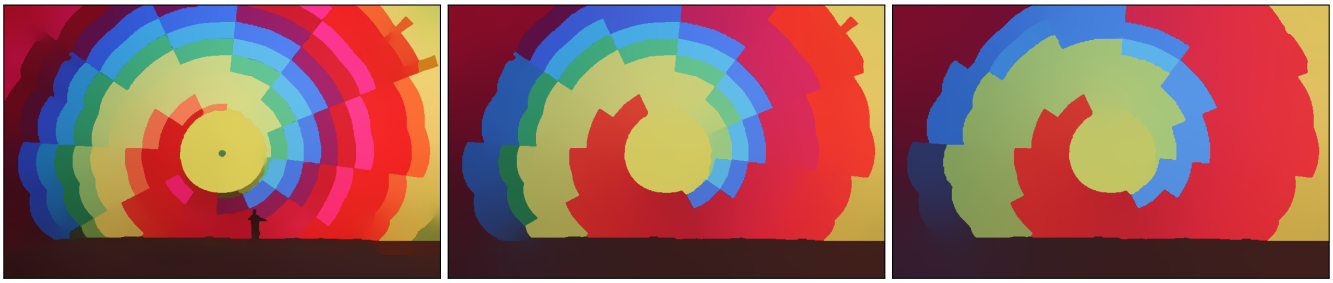

(e) Ours

Figure 16. Examples of the scale space for (a) the input image, constructed by (b) WLS [1] [(from left to right) $\lambda = 3\times10^4, 1\times10^5, 5\times10^5$, $\mu = 40$], (c) WLS [1] [(from left to right) $\lambda = 3 \times 10^2, 2 \times 10^3, 5 \times 10^3$, $\mu = 5$], (d) RGF [11] [(from left to right) $\sigma_s = 10, 20, 40$, $\sigma_r = 0.05$, $k = 5$], (e) our model [$\mathbf{u}^0 = \mathbf{u}_{l_1}$, (from left to right) $\lambda = 1 \times 10^3, 4 \times 10^3, 1 \times 10^4$, $\mu = 5$, $\nu = 40$, $k = 5$].

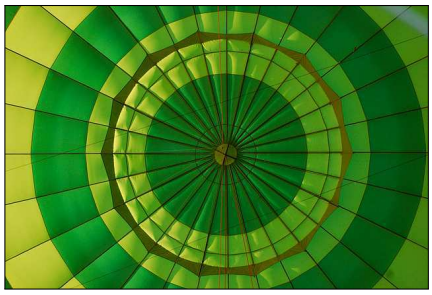

(a) Input image

(b) WLS [1] ($\mu = 40$)

(c) WLS [1] ($\mu = 5$)

(d) RGF [11]

(e) Ours

Figure 17. Examples of the scale space for (a) the input image, constructed by (b) WLS [1] [(from left to right) $\lambda = 5\times10^3, 2\times10^5, 5\times10^6$, $\mu = 40$], (c) WLS [1] [(from left to right) $\lambda = 5 \times 10, 2 \times 10^3, 5 \times 10^4$, $\mu = 5$], (d) RGF [11] [(from left to right) $\sigma_s = 10, 20, 40$, $\sigma_r = 0.05$, $k = 5$], (e) our model [$\mathbf{u}^0 = \mathbf{u}_{l_1}$, (from left to right) $\lambda = 3 \times 10^2, 4 \times 10^3, 1 \times 10^4$, $\mu = 5$, $\nu = 40$, $k = 5$].

(a) Input

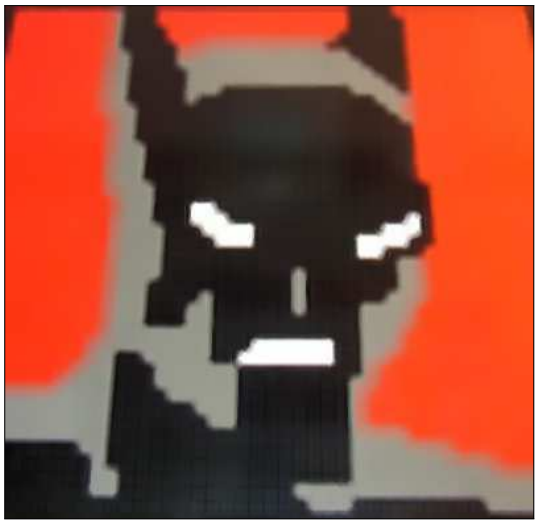

(b) Cov. M1 [4]

(c) RTV [9]

(d) RGF [11]

(e) Ours

Figure 18. Examples of the texture removal for regular textures. (a) Input image, (b) Cov. M1 [4] [$\sigma = 0.3$, $r = 10$)], (c) RTV [9] [$\lambda = 0.01$, $\sigma = 6$], (d) RGF [11] [$\sigma_s = 5$, $\sigma_r = 0.05$, $k = 5$], (e) ours [$\mathbf{u}^0 = \mathbf{u}_{l_1}$, $\lambda = 1000$, $\sigma = 2$, $\mu = 5$, $\nu = 40$, $k = 10$].

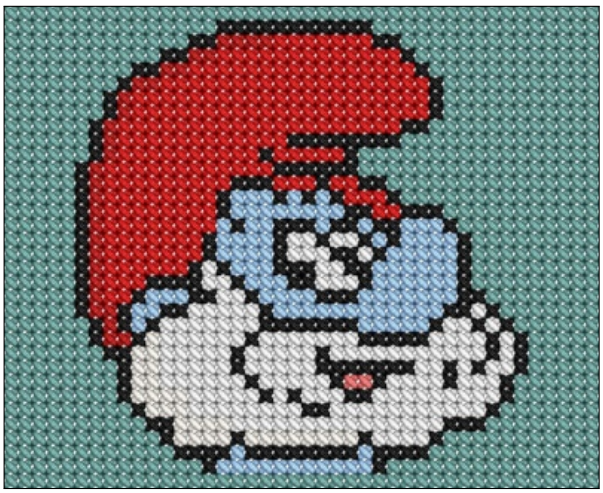

(a) Input

(b) Cov. M1 [4]

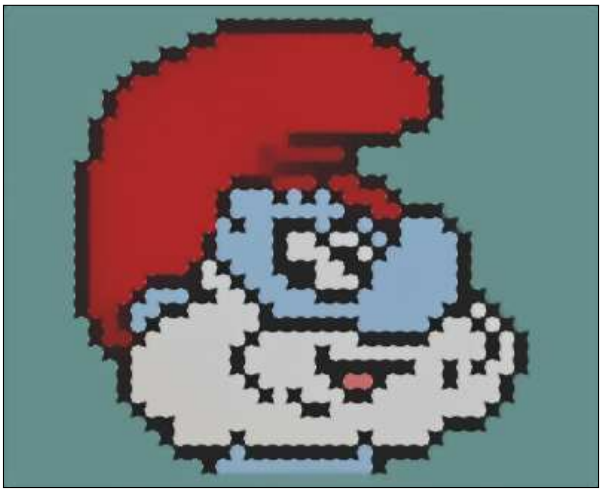

(c) RTV [9]

(d) RGF [11]

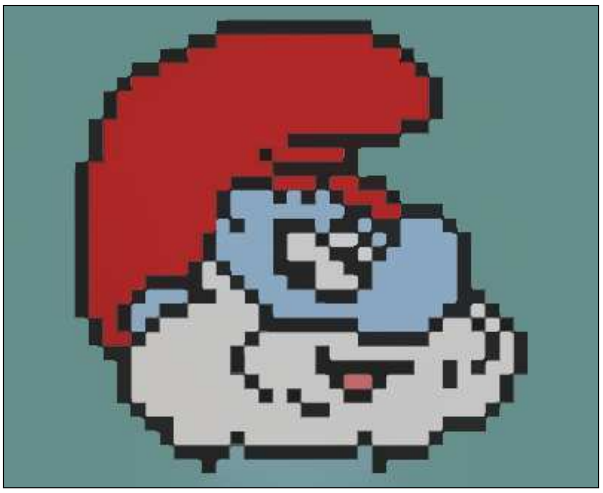

(e) Ours

Figure 19. Examples of the texture removal for regular textures. (a) Input image, (b) Cov. M1 [4] [$\sigma = 0.3$, $r = 10$)], (c) RTV [9] [$\lambda = 0.01$, $\sigma = 6$], (d) RGF [11] [$\sigma_s = 5$, $\sigma_r = 0.1$, $k = 5$], (e) ours [$\mathbf{u}^0 = \mathbf{u}_{l_1}$, $\lambda = 2000$, $\sigma = 2$, $\mu = 5$, $\nu = 40$, $k = 10$].

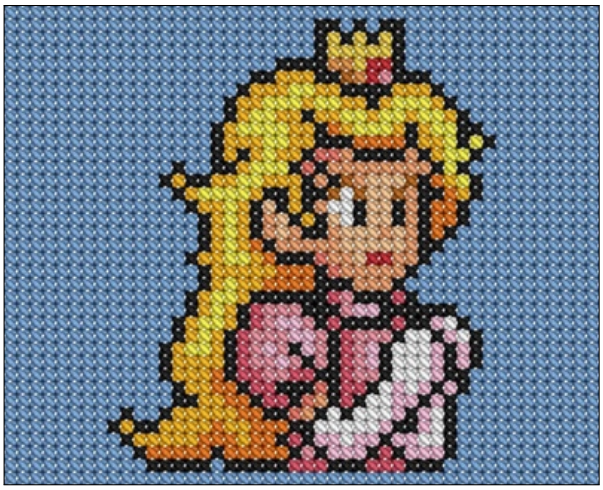

(a) Input

(b) Cov. M1 [4]

(c) RTV [9]

(d) RGF [11]

(e) Ours

Figure 20. Examples of the texture removal for regular textures. (a) Input image, (b) Cov. M1 [4] [$\sigma = 0.3$, $r = 10$)], (c) RTV [9] [$\lambda = 0.01$, $\sigma = 6$], (d) RGF [11] [$\sigma_s = 5$, $\sigma_r = 0.1$, $k = 5$], (e) ours [$\mathbf{u}^0 = \mathbf{u}_{l_1}$, $\lambda = 2000$, $\sigma = 2$, $\mu = 5$, $\nu = 40$, $k = 10$].

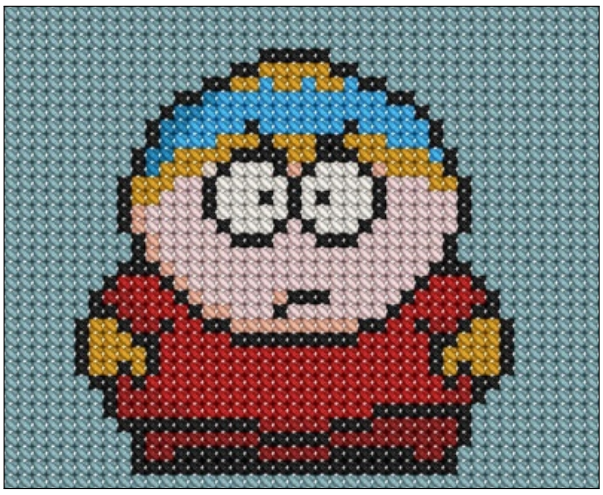

(a) Input

(b) Cov. M1 [4]

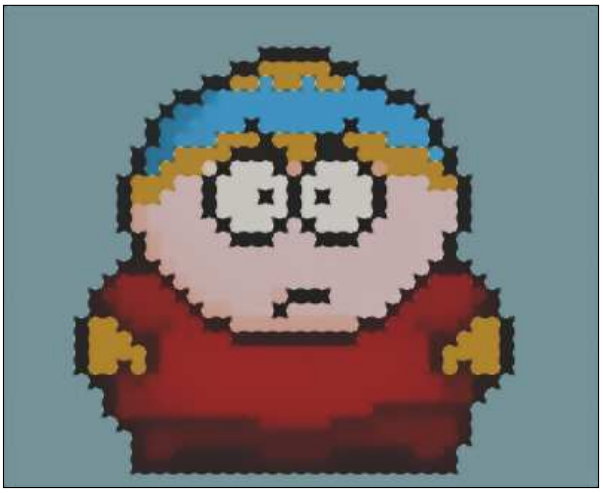

(c) RTV [9]

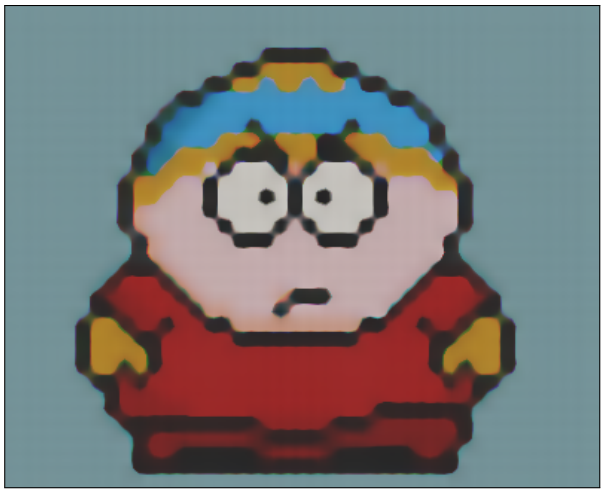

(d) RGF [11]

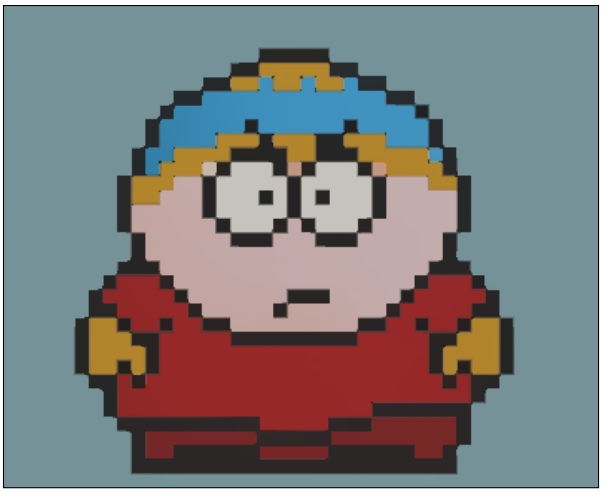

(e) Ours

Figure 21. Examples of the texture removal for regular textures. (a) Input image, (b) Cov. M1 [4] [$\sigma = 0.3$, $r = 10$)], (c) RTV [9] [$\lambda = 0.01$, $\sigma = 6$], (d) RGF [11] [$\sigma_s = 5$, $\sigma_r = 0.1$, $k = 5$], (e) ours [$\mathbf{u}^0 = \mathbf{u}_{l_1}$, $\lambda = 2000$, $\sigma = 2$, $\mu = 5$, $\nu = 40$, $k = 10$].

(a) Input

(b) Cov. M1 [4]

(c) RTV [9]

(d) RGF [11]

(e) Ours

Figure 22. Examples of the texture removal for regular textures. (a) Input image, (b) Cov. M1 [4] [$\sigma = 0.3$, $r = 10$)], (c) RTV [9] [$\lambda = 0.01$, $\sigma = 3$], (d) RGF [11] [$\sigma_s = 3$, $\sigma_r = 0.05$, $k = 5$], (e) ours [$\mathbf{u}^0 = \mathbf{u}_{l_1}$, $\lambda = 2000$, $\sigma = 1$, $\mu = 5$, $\nu = 40$, $k = 10$].

(a) Input

(b) Cov. M1 [4]

(c) RTV [9]

(d) RGF [11]

(e) Ours

Figure 23. Examples of the texture removal for regular textures. (a) Input image, (b) Cov. M1 [4] [$\sigma = 0.3$, $r = 10$)], (c) RTV [9] [$\lambda = 0.01$, $\sigma = 3$], (d) RGF [11] [$\sigma_s = 3$, $\sigma_r = 0.05$, $k = 5$], (e) ours [$\mathbf{u}^0 = \mathbf{u}_{l_1}$, $\lambda = 500$, $\sigma = 1$, $\mu = 5$, $\nu = 40$, $k = 10$].

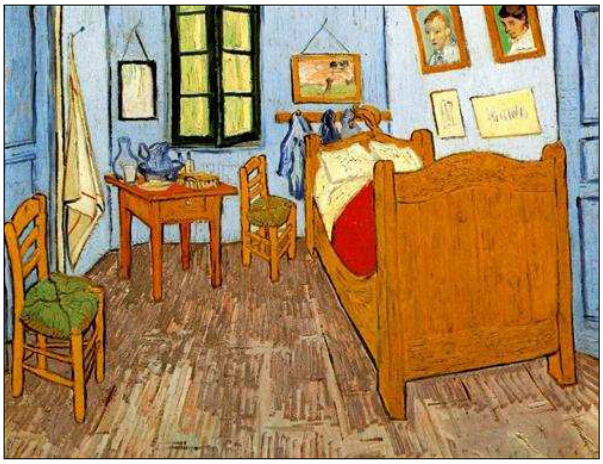

(a) Input

(b) Cov. M1 [4]

(c) RTV [9]

(d) RGF [11]

(e) Ours

Figure 24. Examples of the texture removal for irregular textures. (a) Input image, (b) Cov. M1 [4] [$\sigma = 0.3$, $r = 10$)], (c) RTV [9] [$\lambda = 0.01$, $\sigma = 6$], (d) RGF [11] [$\sigma_s = 3$, $\sigma_r = 0.05$, $k = 5$], (e) ours [$\mathbf{u}^0 = \mathbf{u}_{l_1}$, $\lambda = 50$, $\sigma = 1$, $\mu = 5$, $\nu = 40$, $k = 10$].

(a) Input

(b) Cov. M1 [4]

(c) RTV [9]

(d) RGF [11]

(e) Ours

Figure 25. Examples of the texture removal for irregular textures. (a) Input image, (b) Cov. M1 [4] [$\sigma = 0.3$, $r = 10$)], (c) RTV [9] [$\lambda = 0.01$, $\sigma = 6$], (d) RGF [11] [$\sigma_s = 3$, $\sigma_r = 0.1$, $k = 5$], (e) ours [$\mathbf{u}^0 = \mathbf{u}_{l_1}$, $\lambda = 2000$, $\sigma = 2$, $\mu = 5$, $\nu = 40$, $k = 10$].

(a) Input

(b) Cov. M1 [4]

(c) RTV [9]

(d) RGF [11]

(e) Ours

Figure 26. Examples of the texture removal for irregular textures. (a) Input image, (b) Cov. M1 [4] [$\sigma = 0.3$, $r = 10$)], (c) RTV [9] [$\lambda = 0.01$, $\sigma = 6$], (d) RGF [11] [$\sigma_s = 5$, $\sigma_r = 0.05$, $k = 5$], (e) ours [$\mathbf{u}^0 = \mathbb{1}$, $\lambda = 50$, $\sigma = 2$, $\mu = 5$, $\nu = 40$, $k = 5$].

(a) Input

(b) Cov. M1 [4]

(c) RTV [9]

(d) RGF [11]

(e) Ours

Figure 27. Examples of the texture removal for irregular textures. (a) Input image, (b) Cov. M1 [4] [$\sigma = 0.3$, $r = 10$)], (c) RTV [9] [$\lambda = 0.01$, $\sigma = 9$], (d) RGF [11] [$\sigma_s = 5$, $\sigma_r = 0.05$, $k = 5$], (e) ours [$\mathbf{u}^0 = \mathbb{1}$, $\lambda = 100$, $\sigma = 2$, $\mu = 5$, $\nu = 40$, $k = 5$].

(a) Input

(b) Cov. M1 [4]

(c) RTV [9]

(d) RGF [11]

(e) Ours

Figure 28. Examples of the texture removal for irregular textures. (a) Input image, (b) Cov. M1 [4] [$\sigma = 0.3$, $r = 10$)], (c) RTV [9] [$\lambda = 0.01$, $\sigma = 3$], (d) RGF [11] [$\sigma_s = 3$, $\sigma_r = 0.05$, $k = 5$], (e) ours [$\mathbf{u}^0 = \mathbb{1}$, $\lambda = 50$, $\sigma = 1$, $\mu = 5$, $\nu = 40$, $k = 5$].

(a) Input

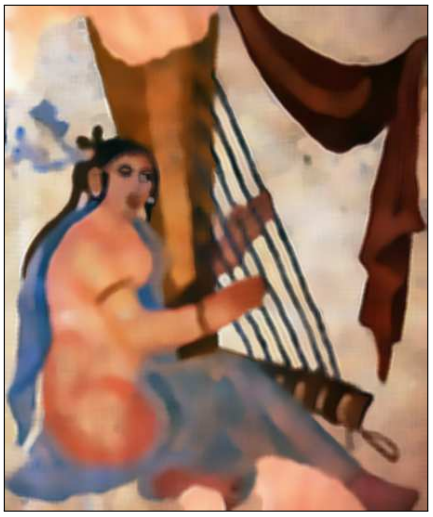

(b) Cov. M1 [4]

(c) RTV [9]

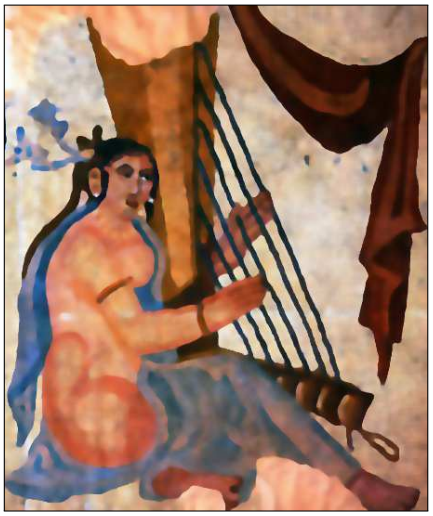

(d) RGF [11]

(e) Ours

Figure 29. Examples of the texture removal for irregular textures. (a) Input image, (b) Cov. M1 [4] [$\sigma = 0.3$, $r = 10$)], (c) RTV [9] [$\lambda = 0.01$, $\sigma = 6$], (d) RGF [11] [$\sigma_s = 3$, $\sigma_r = 0.1$, $k = 5$], (e) ours [$\mathbf{u}^0 = \mathbb{1}$, $\lambda = 50$, $\sigma = 2$, $\mu = 5$, $\nu = 40$, $k = 5$].

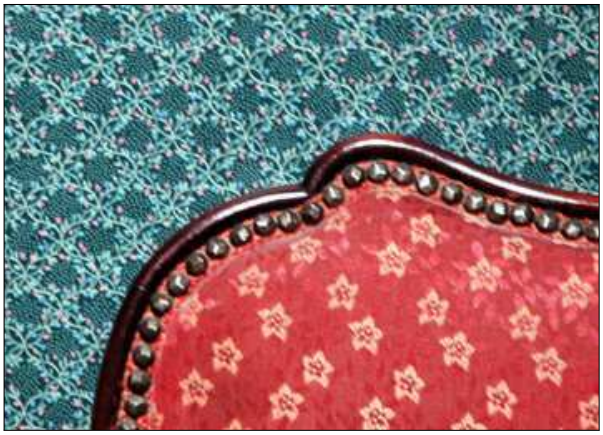

(a) Input

(b) Cov. M1 [4]

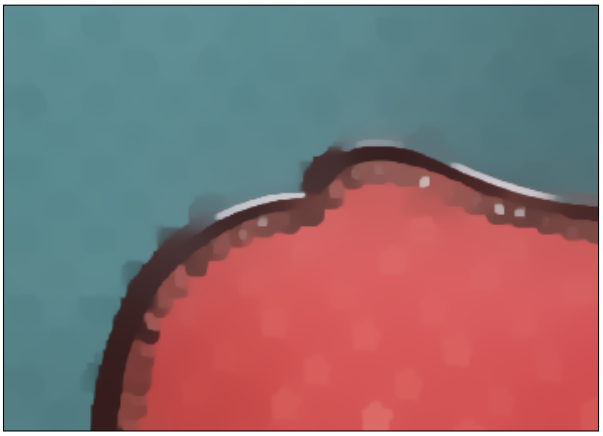

(c) RTV [9]

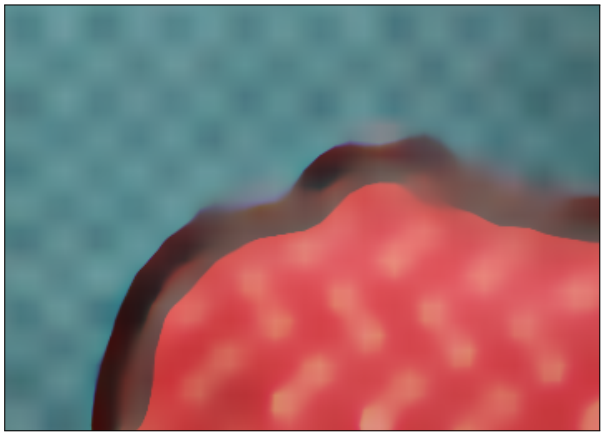

(d) RGF [11]

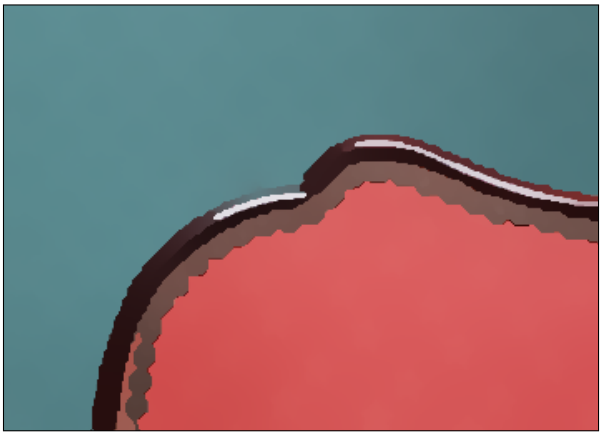

(e) Ours

Figure 30. Examples of the texture removal for irregular textures. (a) Input image, (b) Cov. M1 [4] [$\sigma = 0.3$, $r = 10$)], (c) RTV [9] [$\lambda = 0.05$, $\sigma = 3$], (d) RGF [11] [$\sigma_s = 9$, $\sigma_r = 0.1$, $k = 5$], (e) ours [$\mathbf{u}^0 = \mathbb{1}$, $\lambda = 1000$, $\sigma = 1$, $\mu = 5$, $\nu = 40$, $k = 5$].

(a) RGB image (b) Flash NIR image

(c) GF [3] (d) Ours

Figure 31. RGB and flash NIR image restoration on *teapot* sequence [10]: (a) RGB image, (b) NIR image, (c) GF [3] [$r = 3$, $\varepsilon = 0.0004$], (d) ours [$\mathbf{u}^0 = \mathbb{1}$, $\lambda = 15$, $\mu = 60$, $\nu = 30$, $k = 5$].

(a) RGB image (b) Flash NIR image

(c) GF [3] (d) Ours

Figure 32. RGB and flash NIR image restoration on *books* sequence [10]: (a) RGB image, (b) NIR image, (c) GF [3] [$r = 3$, $\varepsilon = 0.0004$], (d) ours [$\mathbf{u}^0 = \mathbb{1}$, $\lambda = 15$, $\mu = 60$, $\nu = 30$, $k = 5$].

(a) RGB image

(b) Flash NIR image

(c) GF [3]

(d) Ours

Figure 33. RGB and flash NIR image restoration on *window* sequence [10]: (a) RGB image, (b) NIR image, (c) GF [3] [$r = 3$, $\varepsilon = 0.0004$], (d) ours [$\mathbf{u}^0 = \mathbb{1}$, $\lambda = 15$, $\mu = 60$, $\nu = 30$, $k = 5$].

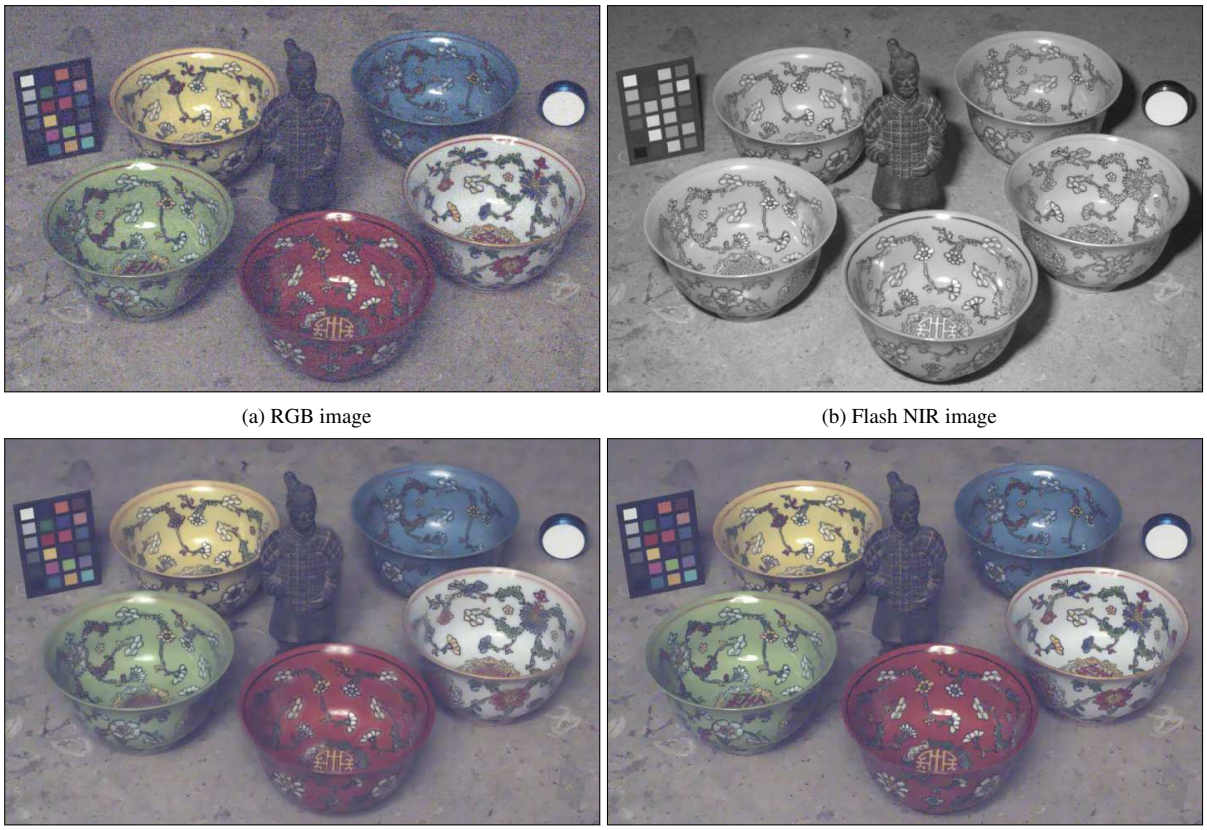

(a) RGB image (b) Flash NIR image

(c) GF [3] (d) Ours

Figure 34. RGB and flash NIR image restoration on *bowls* sequence [10]: (a) RGB image, (b) NIR image, (c) GF [3] [$r = 3$, $\varepsilon = 0.0004$], (d) ours [$\mathbf{u}^0 = \mathbb{1}$, $\lambda = 7$, $\mu = 30$, $\nu = 30$, $k = 5$].

(a) Flash image

(b) Non-flash image

(c) GF [3]

(d) Result of [10]

Ours

Figure 35. Flash and non-flash image restoration on *cave* sequence [7]. (a) Flash image, (b) non-flash image, (c) GF [3] [$r = 3$, $\varepsilon = 0.0004$], (d) result of [10], and (f) ours [$\mathbf{u}^0 = \mathbb{1}$, $\lambda = 15$, $\mu = 60$, $\nu = 30$, $k = 5$]. The results of (d) is obtained from the project webpage.

(a) Flash image

(b) Non-flash image

(c) GF [3]

(d) Result of [10]

Ours

Figure 36. Flash and non-flash image restoration on *pot* sequence [7]. (a) Flash image, (b) non-flash image, (c) GF [3] [$r = 1, \varepsilon = 0.0004$], (d) result of [10], and (f) ours [$\mathbf{u}^0 = \mathbb{1}$, $\lambda = 3$, $\mu = 60$, $\nu = 30$, $k = 5$]. The results of (d) is obtained from the project webpage.